



# Kent Academic Repository

Sun, Caiying, Yan, Yong, Zhang, Wenbiao and Ding, Shao (2024) *Measurement of CO2 leakage from pipelines under CCS conditions through acoustic emission detection and data driven modeling*. *Measurement*. ISSN 0263-2241.

## Downloaded from

<https://kar.kent.ac.uk/106385/> The University of Kent's Academic Repository KAR

## The version of record is available from

<https://doi.org/10.1016/j.measurement.2024.115164>

## This document version

Publisher pdf

## DOI for this version

## Licence for this version

UNSPECIFIED

## Additional information

## Versions of research works

### Versions of Record

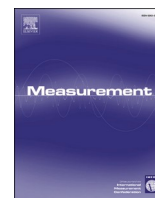
If this version is the version of record, it is the same as the published version available on the publisher's web site. Cite as the published version.

### Author Accepted Manuscripts

If this document is identified as the Author Accepted Manuscript it is the version after peer review but before type setting, copy editing or publisher branding. Cite as Surname, Initial. (Year) 'Title of article'. To be published in **Title of Journal**, Volume and issue numbers [peer-reviewed accepted version]. Available at: DOI or URL (Accessed: date).

### Enquiries

If you have questions about this document contact [ResearchSupport@kent.ac.uk](mailto:ResearchSupport@kent.ac.uk). Please include the URL of the record in KAR. If you believe that your, or a third party's rights have been compromised through this document please see our [Take Down policy](https://www.kent.ac.uk/guides/kar-the-kent-academic-repository#policies) (available from <https://www.kent.ac.uk/guides/kar-the-kent-academic-repository#policies>).



# Measurement of CO<sub>2</sub> leakage from pipelines under CCS conditions through acoustic emission detection and data driven modeling

Caiying Sun<sup>a,b</sup>, Yong Yan<sup>c</sup>, Wenbiao Zhang<sup>a,\*</sup>, Ding Shao<sup>a</sup>

<sup>a</sup> School of Control and Computer Engineering, North China Electric Power University, Beijing 102206, PR China

<sup>b</sup> School of Automation and Electrical Engineering, Inner Mongolia University of Science & Technology, Baotou 014010, PR China

<sup>c</sup> Hangzhou International Innovation Institute, Beihang University, Hangzhou 311115, PR China

## ARTICLE INFO

### Keywords:

Carbon capture and storage  
Data driven models  
Acoustic emission  
Leakage measurement  
Volume fraction of N<sub>2</sub>

## ABSTRACT

CO<sub>2</sub> leakage from carbon capture and storage (CCS) networks may lead to ecological hazards, bodily injury and economic losses. In addition, captured CO<sub>2</sub> often contains impurities which affect the leakage behavior of CO<sub>2</sub>. This paper presents a method for continuous and quantitative measurements of CO<sub>2</sub> leakage flowrate and the volume fraction of impurities by combining data-driven models with acoustic emission (AE) and temperature sensors. Three data-driven models based on artificial neural network (ANN), random forest (RF), and least squares support vector machine (LS-SVM) algorithms are established. The outputs from the three data-driven models are then integrated to give improved results. Experimental work was conducted on a purpose-built CO<sub>2</sub> leakage test rig under a range of conditions. N<sub>2</sub> was injected to the CO<sub>2</sub> gas stream as an impurity medium. Results show that the integrated model yields a relative error within  $\pm 4.0\%$  for leakage flowrate and  $\pm 3.4\%$  for volume fraction of N<sub>2</sub>.

## 1. Introduction

Fossil fuel power generation and other industrial emissions of carbon dioxide are threats to global climate. CCS is one of the important means to alleviate greenhouse gas emissions, especially CO<sub>2</sub> emissions [1–3]. The technology for safe transportation and storage of pressurized liquids or gases has been established for years. These technologies have been well proven in practice, especially in oil and natural gas transportation and storage. In comparison with oil and natural gas, CO<sub>2</sub> poses a number of different risks in the accidental leakage due to its unusual physical properties [4,5]. Potential CO<sub>2</sub> leakages from high-pressure CO<sub>2</sub> transportation pipelines pose significant threat to the safety and health of those living in the vicinity of CCS pipelines. The possibility that CO<sub>2</sub> may leak from transportation pipelines is a primary concern for the safety and effectiveness of the CCS technologies. Permanent, automated monitoring techniques for the continuous leakage measurement of CO<sub>2</sub> from transportation pipelines are necessary [6].

The conventional method for detecting pipeline leakage involves human examination using ground-penetrating radar [7,10]. However, this approach lacks real-time monitoring capabilities, which can lead to increased environmental pollution and financial losses [8]. In recent years, various techniques have been used for real-time monitoring of

pipeline leakage, including infrared thermal imagers [9,10], electromagnetic sensors [11,12] and optical sensors [13,14]. Nevertheless, high-resolution infrared cameras are expensive and not suitable for accurately quantifying small leakages [8,15]. Additionally, electromagnetic sensors can only measure the flowrate of conductive liquids and cannot be used for detecting leakage flowrate of CO<sub>2</sub>. Moreover, the optical method is affected significantly by the on-site environment and cannot accurately measure the leakage flowrate. Consequently, there is a pressing need for CO<sub>2</sub> leakage measurement methods with non-destructive sensing, real-time continuous monitoring, long-distance signal transmission, and high-pressure resistance.

When a continuous leakage occurs from a CO<sub>2</sub> pipeline, due to the pressure difference between the inside and outside of the pipeline, CO<sub>2</sub> emits rapidly from inside to outside through the leakage hole [8], and the AE sensor detects the leakage to generate an acoustic emission signal, and through the subsequent analysis and processing of the signal, leakage measurement is achieved [16,17]. In comparison with other methods, this technique uses only an AE sensor and a temperature transducer, which are low in cost and small in size. Therefore, the AE technique is more cost-effective than other methods.

Various methods have been proposed using acoustic monitoring techniques for CO<sub>2</sub> leakage measurement [18]. Through theoretical

\* Corresponding author.

E-mail address: [wbzhang@ncepu.edu.cn](mailto:wbzhang@ncepu.edu.cn) (W. Zhang).

<https://doi.org/10.1016/j.measurement.2024.115164>

Received 31 January 2024; Received in revised form 17 June 2024; Accepted 18 June 2024

Available online 22 June 2024

0263-2241/© 2024 Elsevier Ltd. All rights reserved, including those for text and data mining, AI training, and similar technologies.

analysis, numerical simulation and experimental validation of AE energy, Cui and Yan *et al.* [19,20] investigated key issues such as leakage source and acoustic wave propagation characteristics, and leakage localisation for CO<sub>2</sub> transport and storage devices. In view of the advantages of the AE technique, there have been some qualitative studies with AE sensors for downhole in wellbore leakage detection. Ishida *et al.* [21] conducted hydraulic fracturing experiments using supercritical CO<sub>2</sub> in a hole drilled into a granitic hot rock at a depth of 7.24 m–7.40 m. A total of 16 AE sensors were arranged around the pressurized section of the underground storage device to record AE events during leakage and analyze the location of leakage sources. Kim *et al.* [22] compared three deep-learning models (MLP, LSTM, and CISM–LSTM) via numerical simulation for predicting the likelihood of CO<sub>2</sub> leakage from a pipeline. Previous studies are mostly concerned with localization of leak points and qualitative analyses of leakage through feature characterization.

Although AE sensors have been applied to locate a CO<sub>2</sub> leakage source from a CCS pipeline [16–21], the leakage flowrate of CO<sub>2</sub> still needs to be quantitatively measured. By combining the AE signal and relevant temperature and pressure data, an estimation model for leakage flowrate monitoring based on machine learning algorithms should be developed to ensure the safe and efficient operation of CCS pipeline networks [6].

Skaugen and Zanobetti [23,24] investigated the impact of CO<sub>2</sub> stream impurities on pipeline transport costs, showed that the level of impurities in the CO<sub>2</sub> mixture may increase the pipeline transport costs by up to 22 %. As a result, the development of reliable quantitative methods for predicting leakage for CO<sub>2</sub> pipelines in the presence of the typical impurities is of significant value [5].

Accidental leakage may occur through a damaged section of the pipeline caused by defects introduced into the pipeline such as mechanical damage, corrosion or material defects, and operational mistakes, for example technical or mechanical breakdowns of equipment and tools (e.g., valves and pumps from pipelines) [5,25–27]. Considerable negative effects and threats could be exerted on the local environment and residents nearby due to the high CO<sub>2</sub> concentration released from the high-pressure pipelines [28,29]. Continuous corrosion may lead to pipeline leakage and the corrosion is due to CO<sub>2</sub> dissolved in water, which then forms carbonic acid (H<sub>2</sub>CO<sub>3</sub>) and reacts with the steel in the pipelines [24,30,31].

CCS capture processes can result in the presence of diverse impurities in CO<sub>2</sub> flow stream, including but not limited to CH<sub>4</sub>, H<sub>2</sub>O, H<sub>2</sub>S, SO<sub>x</sub>, NO<sub>x</sub>, N<sub>2</sub>, O<sub>2</sub>, glycol, and other substances [31]. As a common and non-toxic impurity [32], N<sub>2</sub> is used in this study as a test medium to investigate the effect of different content of impurity gas on acoustic emission signals and temperature changes. The contribution of this article is to propose a method to measure CO<sub>2</sub> gas leakage from a CCS pipeline, and develop an integrated data-driven model with multiple feature parameters from different sensors as inputs to predict the leakage flowrate of CO<sub>2</sub> gas and the volume fraction of impurity gas N<sub>2</sub> under CCS

conditions.

## 2. Methodology

### 2.1. Measurement strategy

The strategy of the proposed measurement method is shown in Fig. 1. The strategy is realized through soft computing and data-driven modeling. The artificial neural network (ANN), random forest (RF), and least squares support vector machine (LS-SVM) algorithms have performed well in data-driven modelling for predicting the fluid flowrate in earlier research [6,33–36]. A method that integrates these three algorithms is proposed in this paper to measure the leakage flowrate of CO<sub>2</sub> and the volume fraction of impurity gas N<sub>2</sub>. In this approach only an AE sensor and a temperature transducer are used to acquire signals from the pipeline. It should be pointed out that the signal from the AE sensor contains information about the pressure variations in the pipeline, so no separate pressure transducer is required in the sensing system.

### 2.2. Inputs for data-driven models

It has been shown that among the commonly used time-domain characteristic parameters (peak amplitude, raise time, energy, ring count, and threshold value) of an acoustic emission signal, the peak amplitude and energy can better characterise experimental objects, such as leakage localization [19,20]. The peak amplitude is the maximum amplitude of the time-domain signal waveform of acoustic emission, which is not affected by the threshold voltage. The strength of the acoustic emission event can be intuitively judged from the peak amplitude and can therefore be used to quantitatively characterise the degree of CO<sub>2</sub> leakage. Energy, as a statistical measure of a sensor signal, is inherently related to other characteristic parameters and can comprehensively reflect the strength of the signal. In this paper, the peak amplitude and energy from different frequency bands are used to analyse the AE signal. The spectrum of the AE signal can also reflect the characteristics of the AE source to a certain extent [37]. This paper extracts the power spectral density (PSD) [38] of the AE signal. The peak frequency of the PSD is taken as one of the characteristic parameters for quantifying CO<sub>2</sub> leakage.

Several features are extracted from the raw AE signals: (1) peak amplitude in the time domain. (2) peak frequency from the PSD. (3) AE energy. Meanwhile, by measuring the temperature of the leakage process in real time, the temperature drop before and after the leakage from the temperature transducer is extracted. The temperature drop, together with the three characteristic parameters from the AE sensor, are used as inputs to the data-driven model to monitor the CO<sub>2</sub> leakage.

### 2.3. Data driven models

A back propagation (BP) ANN model is used to predict the leakage

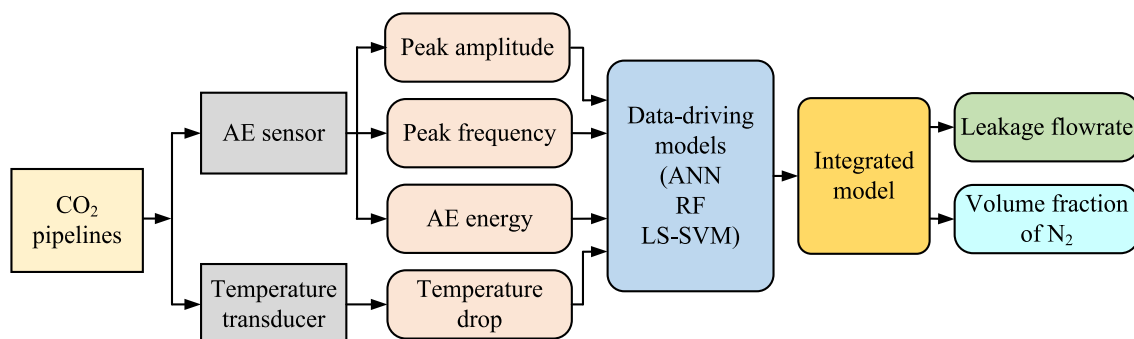


Fig. 1. Overall strategy for CO<sub>2</sub> leakage measurement.

flowrate of CO<sub>2</sub> and the volume fraction of N<sub>2</sub>. The ANN model is a multi-layer feedforward network trained by the error backpropagation algorithm. The structure of BP-ANN is shown in Fig. 2, the model adjusts the weights  $\omega$  and thresholds  $a$  and  $b$  along the negative gradient descent direction to minimize the error between the input and output vectors of the training set. The inputs to the model are  $x_1$ – $x_4$ , which are peak amplitude, peak frequency, AE energy and temperature drop. The outputs are  $y_{BP1}$  and  $y_{BP2}$  as predicted values for the leakage flowrate and the volume fraction of impurity gas N<sub>2</sub>. After repeated training and comparison, the appropriate number of hidden layer neurons is 4, and the appropriate structure of the BP-ANN model is 4: 4: 2. The Tansig function is chosen as an activation function because of its excellent performance in nonlinearity, differentiability, and monotonicity [34]. The algorithm stops iterating when the prediction accuracy reaches the minimum error requirement. The BP-ANN model is advantageous in nonlinear mapping and generalization and can thus approximate complex nonlinear relationships between input and output data.

The RF algorithm uses decision trees as basic models and introduces two random processes: random sampling and random feature selection, to generate multiple decision trees. The structure of RF is shown in Fig. 3, the final ensemble prediction result is obtained by averaging the prediction results of the basic models. Due to the independent physical construction process of each decision tree in the RF, parallel computing is readily implemented to improve the training speed. Meanwhile, the RF model not only avoids overfitting issues but also enhances the prediction accuracy [39].

Fig. 4 shows the structure of LS-SVM, where  $y_{LS-SVM1}$  and  $y_{LS-SVM2}$  are the prediction results of the model,  $a$  is the Lagrange multipliers,  $b$  is bias and  $K$  is the kernel function [33]. A radial basis function (RBF) is chosen as the kernel function here due to the strong non-linear mapping abilities. In the LS-SVM model, the role of RBF kernel is to map low dimensional data to a high-dimensional space and obtain prediction results through weighted summation. Meanwhile, the LS-SVM model has strong generalization capability and robustness, which can better handle noise and nonlinear problems.

For the above three models, the mean relative error (MRE) is used as the evaluation index of the accuracy, which is given as follows,

$$MRE = \frac{1}{n} \sum_{i=1}^n \left| \frac{\hat{y}_i - y}{y} \right| \quad (1)$$

where  $y$  is the desired value of the target variable,  $\hat{y}_i$  is the predicted value for a given model, and  $n$  is the number of validation data samples.

The final result is obtained by combining the outputs from the three individual models,

$$\hat{y} = \frac{1}{3} (y_{BP-ANN} + y_{RF} + y_{LS-SVM}) \quad (2)$$

where  $\hat{y}$  is the prediction result from the integrated model,  $y_{BP-ANN}$ ,  $y_{RF}$  and  $y_{LS-SVM}$  are the prediction results from the BP-ANN, RF and LS-SVM models, respectively. It should be pointed out that the three models are all supervised machine learning models with each model trained independently. From a physical meaning perspective, the selected input variables to the models are from the AE and temperature sensors, which are all correlated with the physical properties of CO<sub>2</sub> leakage. Meanwhile, due to their different data-driven modeling principles, the models have different sensitivities to the same dataset, resulting in different predictive performance. Averaging the outputs of the three models effectively reduces overall variance and bias, avoids overfitting in the individual models, and thus improves the accuracy of the final predicted output. Moreover, the usage of the combined model improves the robustness by reducing the spread or dispersion of the model outputs.

In the present study straightforward averaging of the outputs from the three models is conducted instead of weighted averaging of the three. Further research is required in future under a wider range of leakage conditions, including trials of the developed method on actual CCS systems to assess if the weighted averaging method should be deployed for predicting leakage.

### 3. Experimental setup and conditions

The experimental CO<sub>2</sub> platform used in this study is shown in Fig. 5. The leakage experiments were carried out for different initial pressures and volume fractions of impurity gas N<sub>2</sub>. The CO<sub>2</sub> gas was set to leak into the atmosphere through a vent valve. Since the initial pressure at the test section is up to 5.7 MPa, opening holes on the test platform is dangerous and irreversible. An electric control valve was thus used to control the pipeline leakage and hence the leakage of CO<sub>2</sub> under CCS conditions. The CO<sub>2</sub> storage column is shown in Fig. 6(a), which mainly includes a storage tank and a pressure gauge for measuring gas pressure inside the tank. Figs. 5 and 6(b) depict that the vent valve is installed on the 25 mm bore CO<sub>2</sub> pipeline made from 304 stainless steel. During the experiments the leakage valve was opened from 1 % to 10 % with an increment of 1 %. Along the release pipeline, an AE sensor was installed 20 cm from the valve. The AE sensor (SR40M, Softland) has a bandwidth of 15 ~ 70

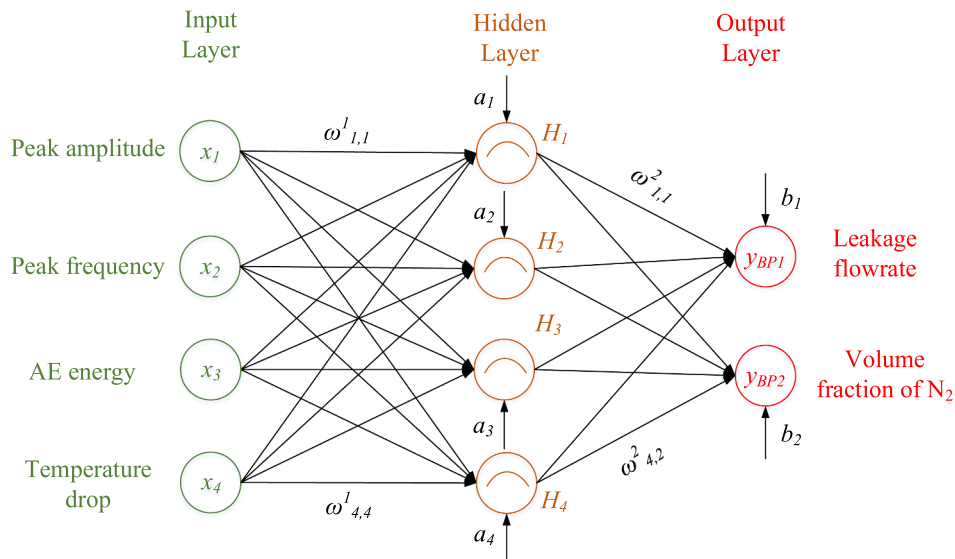


Fig. 2. Structure of the BP-ANN model.

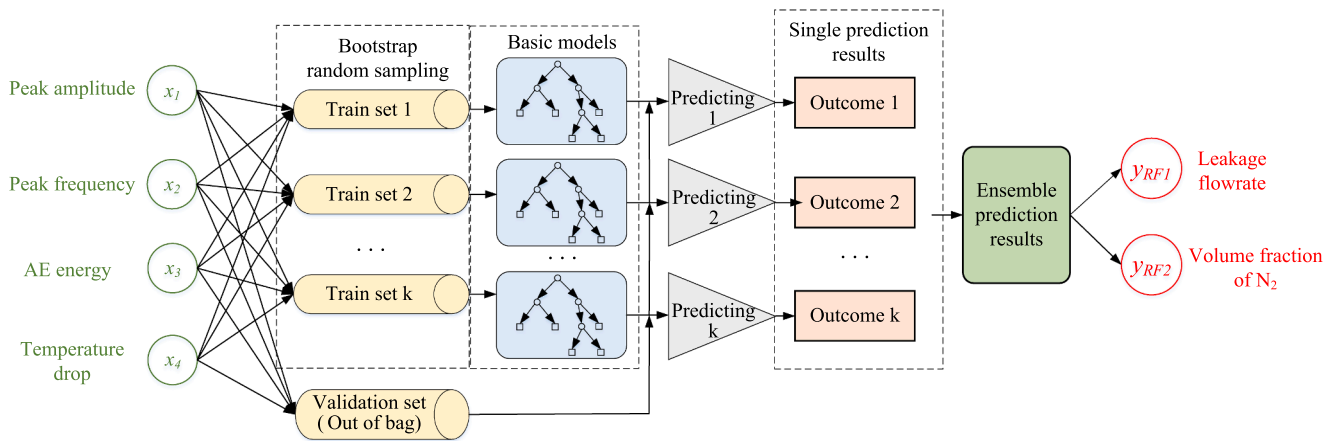


Fig. 3. Structure of the RF model.

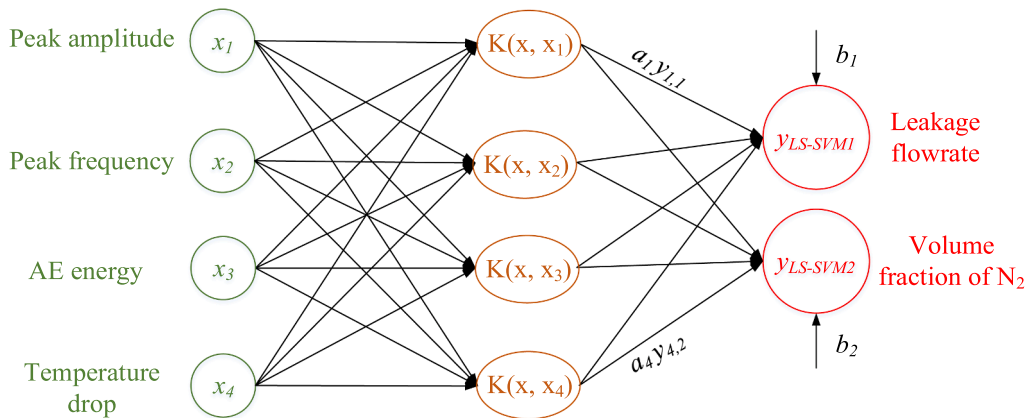


Fig. 4. Structure of the LS-SVM model.

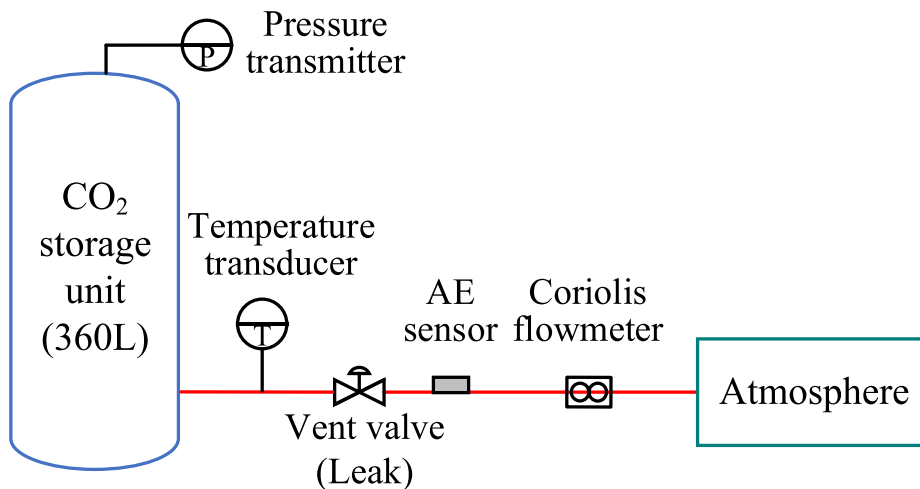


Fig. 5. Schematic of the CO<sub>2</sub> test platform.

kHz. The AE signal is amplified via a linear voltage amplifier with a gain of 40 dB.

The point to surface converter (Fig. 6(b)) is made of solid metal and the surface of the AE sensor is attached to the larger surface of the converter, while the smaller surface is attached to the pipeline. The converter converts pipeline vibration into surface vibration, which is

then collected by the AE sensor. Since it is difficult to distinguish the CO<sub>2</sub> leakage with and without impurities only using AE signals, a temperature transducer is also incorporated to investigate the effect of impurity gases in the pipeline on the leakage temperature.

Several tests were conducted to investigate the release behaviors of CO<sub>2</sub> with and without the impurity gas. A volume fraction of N<sub>2</sub> ranging

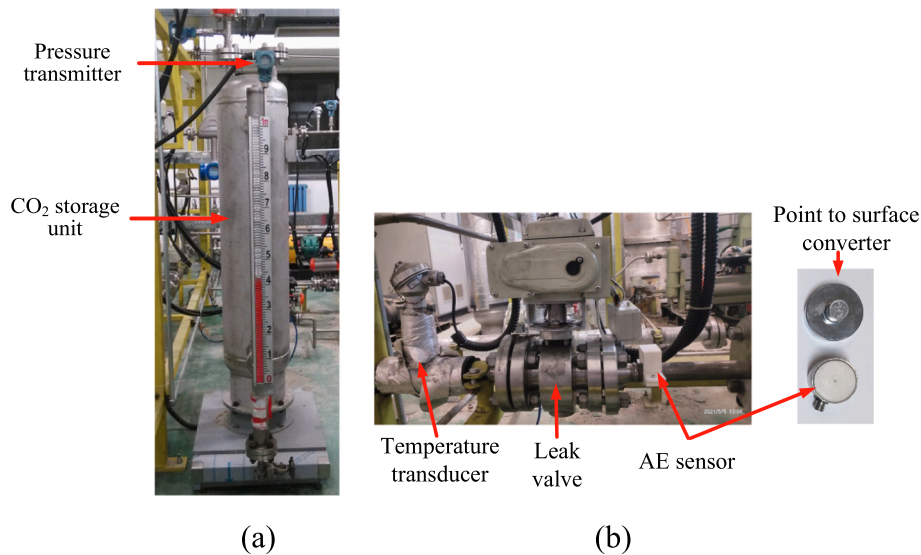


Fig. 6. Photos of the experimental setup. (a) CO2 storage column. (b) Leakage valve and sensors.

from 2 % ~ 30 % was injected into the CO<sub>2</sub> stream to observe the effect of N<sub>2</sub> on the AE signal and temperature characteristics. The gas sources with different CO<sub>2</sub>-N<sub>2</sub> ratios at the storage column determined the volume fraction of N<sub>2</sub>. The resulting gas volume fraction of CO<sub>2</sub> was between 70 % and 100% with an initial pressure from 3 to 5.7 MPa and an initial temperature 18°C.

The actual (reference) leakage flowrate of CO<sub>2</sub> was measured with a Coriolis mass flowmeter (Fig. 5). When the initial temperature (18°C) and pressure in the pipeline were the same, the same actual leakage flowrate was obtained at the same opening of the leakage valve, as shown in Table 1. It should be noted that the CO<sub>2</sub> leakage flowrate varies under different initial pressures and increases with the initial pressure.

The minimum CO<sub>2</sub> leakage that can be measured in the current experimental setup is 12 kg/h, as shown in Table 1. The minimum volume fraction of N<sub>2</sub> in this study is 2 %. According to reference [23], impurity level below 2 % does not affect the cost and operation of pipelines in CCS.

#### 4. Results and discussion

##### 4.1. AE signals

The AE signal without CO<sub>2</sub> leakage is plotted in Fig. 7. The amplitude of the signal is no more than 25 mV. As shown in Fig. 8, when a gas leakage occurs, the amplitude of the signal reaches its peak amplitude of about 5 V quickly at the initial stage. As the time goes by, the oscillation amplitude of the signal decreases and tends to stabilize. The peak amplitude can be used to quantitatively represent the degree of CO<sub>2</sub> leakage.

Fig. 9 show the variations in the peak amplitude of the AE signal during pure CO<sub>2</sub> leakage and CO<sub>2</sub> with 2 % N<sub>2</sub> leakage when the leakage

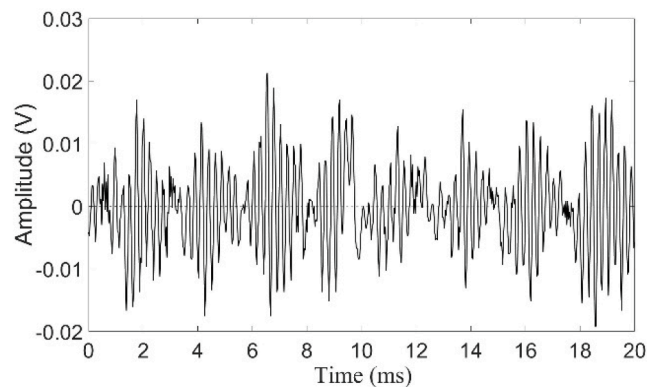


Fig. 7. Typical AE signal waveform without leakage.

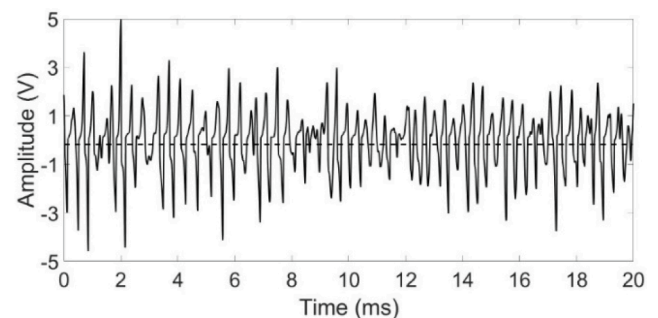


Fig. 8. AE signal waveform during leakage.

Table 1

Actual leakage flowrate under different valve openings.

Valve opening	Leakage flowrate (kg/h)									
	1%	2%	3%	4%	5%	6%	7%	8%	9%	10%
Initial pressure (MPa)										
3.0	12	20	29	38	43	56	71	78	86	100
4.0	17	27	42	63	75	92	105	117	130	140
5.0	20	46	64	80	95	120	125	137	151	170
5.7	24	47	65	87	110	123	145	175	197	220

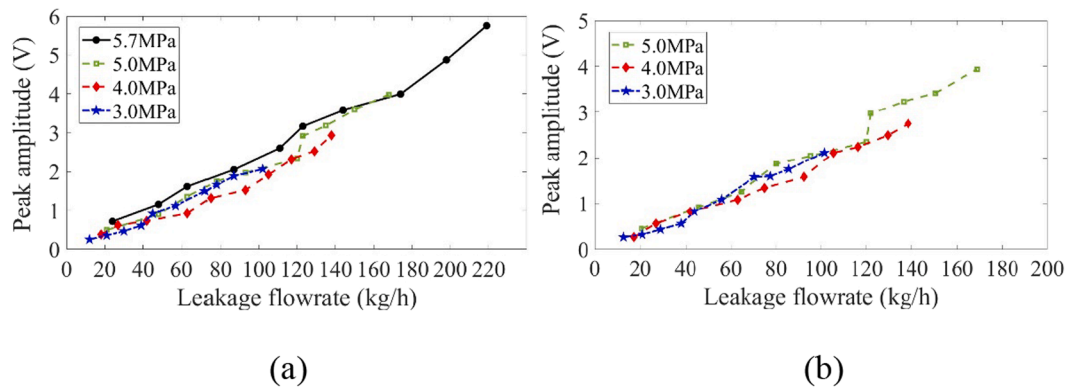


Fig. 9. Relationship between the peak amplitude of the AE signal and the leakage flowrate. (a) Pure CO<sub>2</sub> leakage. (b) CO<sub>2</sub> leakage with 2% N<sub>2</sub> leakage.

flowrate increases gradually. As can be seen, at the same initial pressure, the higher the leakage flowrate, the higher the peak amplitude. In addition, a higher the initial pressure results in a greater pressure difference between the inside and outside of the leakage pipeline, which also produces a higher peak amplitude. The peak amplitude of CO<sub>2</sub> with N<sub>2</sub> leakage presents a similar trend with pure CO<sub>2</sub> leakage, demonstrating high correlation between the leakage flowrate and the peak amplitude.

Figs. 10 and 11 exhibit the normalized PSD of the AE signal at leakage flowrates of 20 kg/h and 170 kg/h. Based on the normalised PSD of the AE signal in each set of experiments, the peak frequency between 40 kHz and 60 kHz is extracted. The sampling frequency used in the data acquisition of the AE signal is 200 kHz with a length of 1024 data points. The frequency resolution in the PSD is thus 0.2 kHz. In the four sets of leakage experiments (Figs. 10 and 11), the peak frequencies are identified as 51.1 kHz, 50.0 kHz, 45.8 kHz and 45.2 kHz. It can be seen that the peak frequencies correspond to the CO<sub>2</sub> leakage flowrate. When the leakage flowrate and initial pressure are the same, similar peak frequencies of AE signals are observed. The molecular weight of N<sub>2</sub> is relatively low, which leads to a reduction in the peak frequency of CO<sub>2</sub> with N<sub>2</sub>, compared to pure CO<sub>2</sub> under the same experimental conditions.

Fig. 12 shows the variations in the peak frequency of the AE signal as the leakage flowrate increases during pure CO<sub>2</sub> leakage at different pressures. Since the valve is used to replicate the leak hole, the leakage flowrate increases with the size of the hole when the initial pressure is constant. When the size of the leakage hole is smaller, the velocity of the fluid at the leakage is higher, generating a higher peak frequency. It can be seen from Fig. 12 that the peak frequency decreases with the leakage flowrate. Experimental results of CO<sub>2</sub> with N<sub>2</sub> impurity yield similar conclusions.

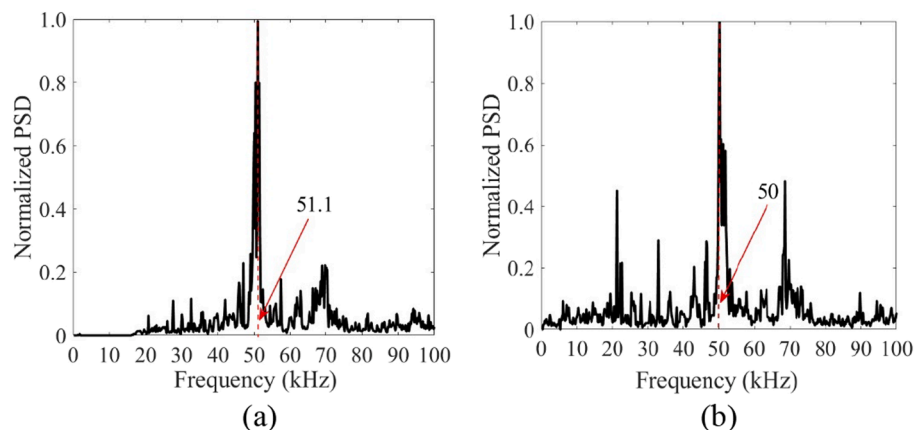


Fig. 10. Normalized PSD of the AE signal for leakage flowrate of 20 kg/h. (a) Pure CO<sub>2</sub> leakage at 5 MPa. (b) CO<sub>2</sub> leakage with 2% N<sub>2</sub> leakage at 5 MPa.

Fig. 13 shows the AE energy distribution during pure CO<sub>2</sub> leakage for three different leakage flowrates. Five band-pass digital filters are used to extract the components in five frequency bands, 0–20 kHz, 20–40 kHz, 40–60 kHz, 60–80 kHz and 80–100 kHz.

It can be seen from Fig. 13 that, with the increase of leakage flowrate (size of leakage holes), the proportion of low-frequency components increases, while the proportion of high-frequency components decreases. Fig. 13(a) indicates that the AE signal due to a small opening of the valve (e.g. 1 %) is weak, but the frequency is relatively high. In contrast, the AE signal from a larger opening (e.g. 10 %) has a stronger amplitude but lower frequency, as shown in Fig. 13(c).

Fig. 14 shows that the AE energy increases with the leakage flowrate and leakage pressure for pure CO<sub>2</sub> leakage and CO<sub>2</sub> with 20 % N<sub>2</sub>. When the volume fraction of impurity gas N<sub>2</sub> is high, a significant impact is seen on the energy of the AE signal. The higher the volume fraction of N<sub>2</sub>, the lower density of the mixture gas, and hence the lower AE energy generated from leakage.

#### 4.2. Temperature drop

As a result of a leakage, the expanded CO<sub>2</sub> and N<sub>2</sub> results in a temperature drop of CO<sub>2</sub> fluid and the surrounding air. Fig. 15 shows the gas temperature evolutions during pure CO<sub>2</sub> leakage and CO<sub>2</sub> with 2 % N<sub>2</sub> leakage when the flowrate is 20 kg/h and 170 kg/h, respectively. Clearly, the temperature variations at the leakage hole shows a similar trend which can be divided into two main stages: a rapid reduction stage and a slowly increasing stage. The sudden onset of the leakage results in a rapid drop in the gas temperature in the pipeline. As the leakage valve is closed at 20 s, the gas temperature begins to rise slowly. The lowest point of the temperature occurs a few seconds after the valve is closed.

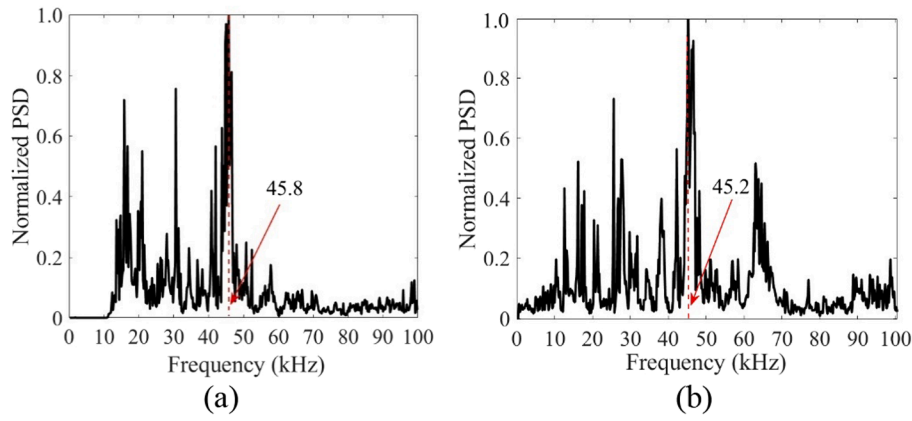


Fig. 11. Normalized PSD of the AE signal for leakage flowrate of 170 kg/h. (a) Pure CO<sub>2</sub> leakage at 5 MPa. (b) CO<sub>2</sub> leakage with 2% N<sub>2</sub> leakage at 5 MPa.

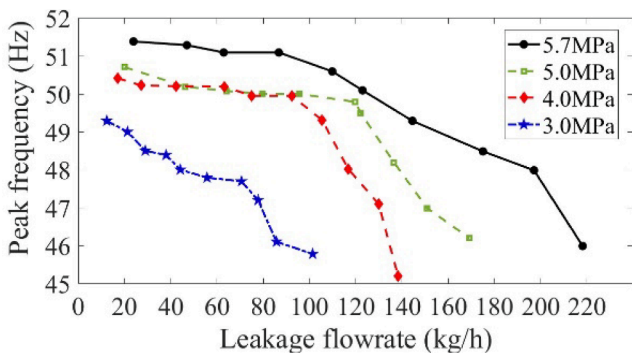


Fig. 12. Relationship between the peak frequency of the AE signal and leakage flowrate of pure CO<sub>2</sub>.

The presence of N<sub>2</sub> accelerates the rate of temperature reduction during the temperature drop.

At the start of a sudden leakage, pressurized CO<sub>2</sub> is released rapidly from the leaking point and experiences an explosive expansion. The expanded CO<sub>2</sub> from the leakage results in a rapid temperature drop of CO<sub>2</sub> fluid itself and the surrounding air [27], and the CO<sub>2</sub> near the leakage point remains in the gaseous phase. Under fixed temperature and pressure conditions, the density of the mixed gas is related to its composition. The higher the volume fraction of N<sub>2</sub> in the mixed gas, the lower the density, and the greater the temperature drop of CO<sub>2</sub> with impurity gas [28,32]. Therefore, the temperature drop due to CO<sub>2</sub> leakage depends on the volume fraction of N<sub>2</sub>, i.e. the temperature drop become pronounced when more N<sub>2</sub> is in the mixture [28]. The

installation position of the thermocouple is very close to the leakage hole, which also causes a greater temperature drop of the gas inside the pipeline when the leakage occurs.

The initial temperature (18°C) minus the measurement of the temperature transducer during the leakage is the temperature drop. Fig. 16 shows the maximum temperature drop for pure CO<sub>2</sub> leakage and CO<sub>2</sub> with N<sub>2</sub> leakage under different leakage flowrates. There are two physical reasons for the temperature drop in Fig. 16. Firstly, a higher leakage flowrate leads to a greater expansion of the medium volume and hence a greater temperature drop. Secondly, a higher N<sub>2</sub> content results in a lower density of the leakage mixture and hence a greater temperature drop.

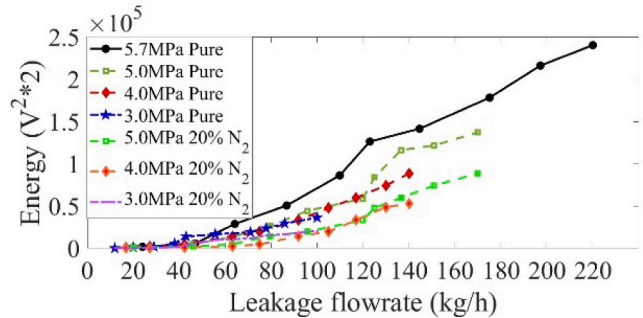


Fig. 14. Relationship between the AE energy and leakage flowrate for pure CO<sub>2</sub> and CO<sub>2</sub> with 20% N<sub>2</sub> leakage.

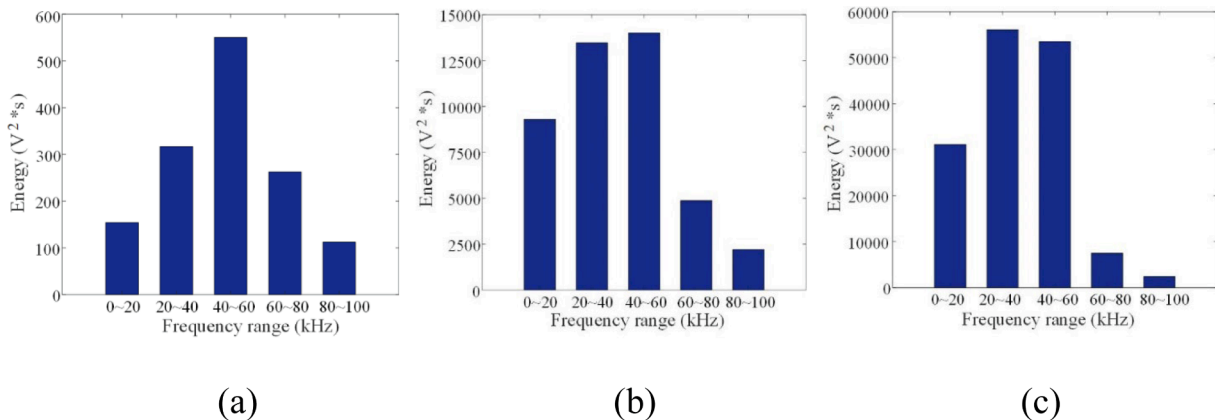


Fig. 13. AE energy distribution for pure CO<sub>2</sub> leakage. (a) leakage flowrate of 20 kg/h. (b) leakage flowrate of 100 kg/h. (c) leakage flowrate of 170 kg/h.

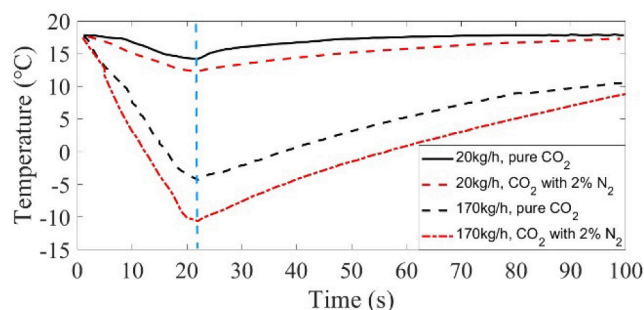


Fig. 15. Temperature evolutions of pure CO<sub>2</sub> leakage and CO<sub>2</sub> with 2 % N<sub>2</sub> leakage under a pressure of 5.0 MPa.

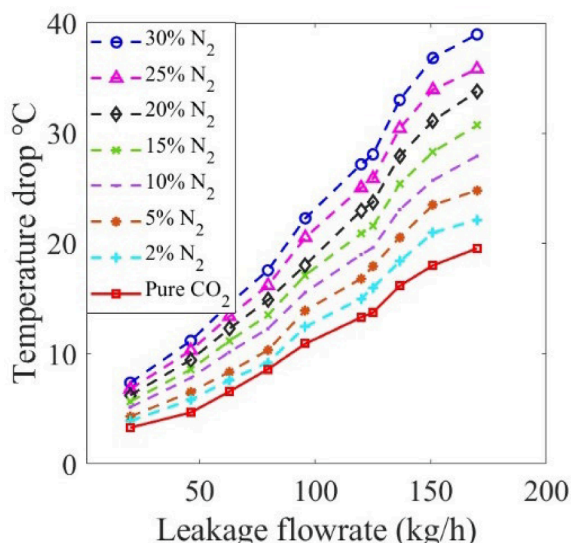


Fig. 16. Relationship between the temperature drop and flowrate of pure CO<sub>2</sub> leakage and CO<sub>2</sub> with N<sub>2</sub> leakage under the pressure of 5.0 MPa.

### 4.3. Leakage flowrate and volume fraction of N<sub>2</sub>

Current industrial standards for CO<sub>2</sub> leakage from pipelines, namely, ISO 27913:2016, ISO/TR 27921:2020 and GB/T 42797-2023 [40–42], do not indicate how much leakage is allowed. There is also no any indication of required detection accuracy. In this study, the minimum leakage rate is set to 12 kg/h. Reference instruments on the CO<sub>2</sub> test platform were used to obtain reference data to evaluate the accuracy of the proposed method. There are a total of 250 data samples used for data-driven models to predict the CO<sub>2</sub> leakage flowrate and volume fraction of N<sub>2</sub>. In the training data, the leakage flowrate ranges from 12 kg/h to 220 kg/h and the volume fraction of N<sub>2</sub> changes from 2 % to 30 %. The optimal predictive model is obtained using a ten-fold cross validation method, and the MRE calculated from 10 validations is used as the evaluation index for predictive models. 20 sets of experimental data are selected as test data samples to predict the CO<sub>2</sub> leakage flowrate and volume fraction of N<sub>2</sub> by four characteristic parameters with the leakage flowrate of 12–170 kg/h and the N<sub>2</sub> content of 2 %–30 %, respectively.

Table 2 indicates that the relative errors of the predicted leakage flowrate of CO<sub>2</sub> and volume fraction of N<sub>2</sub>. Among the three data-driven models, the BP-ANN model yields a relative error in the leakage flowrate within ±5.3 % and a relative error in the N<sub>2</sub> volume fraction within ±4.0 %. The RF model produces corresponding relative errors of ±5.5 % and ±4.3 %, respectively. The LS-SVM model predicts the leakage flowrate within ±4.3 % and N<sub>2</sub> volume fraction within ±3.6 %, respectively. The integrated model performs the best, giving the leakage

Table 2

Range of relative errors of the predicted leakage flowrate and N<sub>2</sub> volume fraction from the established models.

Models	CO <sub>2</sub> leakage flowrate	N <sub>2</sub> volume fraction
BP-ANN	±5.3 %	±4.0 %
RF	±5.5 %	±4.3 %
LS-SVM	±4.3 %	±3.6 %
Integrated model	±4.0 %	±3.4 %

flowrate within ±4.0 % and N<sub>2</sub> volume fraction within ±3.4 %, respectively.

Fig. 17 shows the MREs of the leakage flowrate and volume fraction of N<sub>2</sub> using the three models and the integrated models. The MRE of the leakage flowrate from the BP-ANN model is 1.7 %, and the MRE of N<sub>2</sub> volume fraction is 1.5 %. Similarly, the MRE of the leakage flowrate and N<sub>2</sub> volume fraction from the RF model is 1.8 % and 1.3 %, respectively. The MRE of the leakage flowrate from the LS-SVM model is 1.4 %, and that of N<sub>2</sub> volume fraction is 1.2 %. For the integrated model, the MRE are 1.0 % and 1.1 %, respectively. Fig. 17 indicates that the integrated model has effectively reduced the MRE further in both cases.

Fig. 18 shows the relative errors of the predicted leakage flowrate using all four models for the testing data. With the opening of the valve, the leakage flowrate increases, the sensors can detect a more pronounced AE signal, and the error decreases. It is evident that the data-driven models based on different working principles give different performances for the same leakage flowrate. Among them, the results from the LS-SVM model is slightly better than those from the ANN and RF models. The integrated model outperforms all three individual models.

Fig. 19 shows the relative errors in predicting the volume fraction of N<sub>2</sub> using the four models for the testing data. It is clear that the integrated model yields the lowest error in most cases throughout the range of volume fraction of N<sub>2</sub> from 2 % to 30 %. If only one model is to be used in the data driving modelling, the LS-SVM model is a preferred option as it outperforms the other two individual models.

## 5. Conclusions

In this paper, the leakage flowrate of CO<sub>2</sub> gas from a pipeline and the volume fraction of impurity N<sub>2</sub> in the CO<sub>2</sub> are measured continuously under CCS conditions. The measurement results have suggested that CO<sub>2</sub> leakage can be well characterised using characteristic parameters, which are extracted from the signals of the AE and temperature sensors. Moreover, the results have indicated that the temperature drop is the most sensitive to changes in the volume fraction of impurity gas in the CO<sub>2</sub>. It has also been found that the integrated model by averaging the

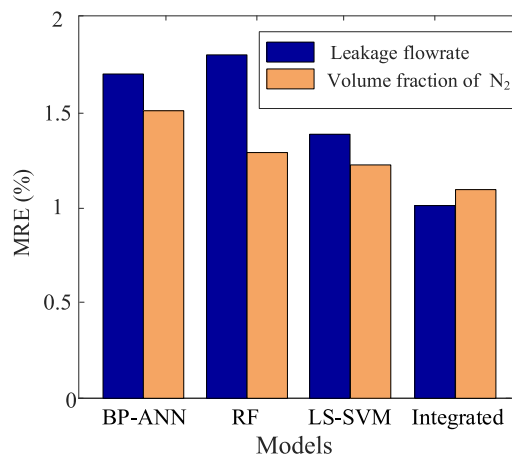


Fig. 17. MRE of the leakage flowrate and the volume fraction of N<sub>2</sub> for the four models.

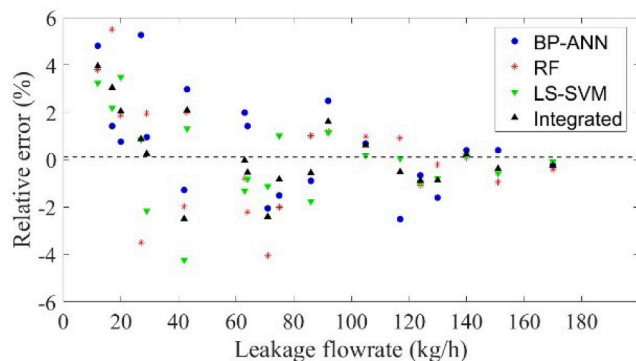


Fig. 18. Relative errors of the leakage flowrate for the four models.

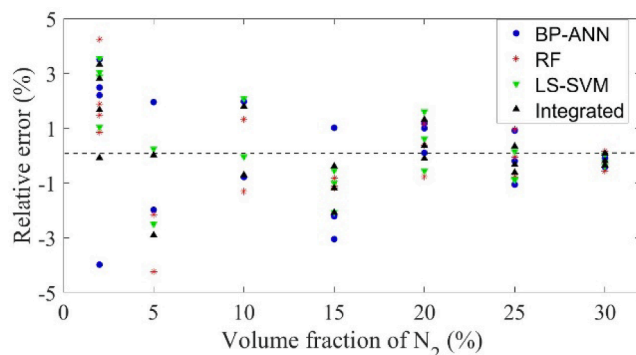


Fig. 19. Relative errors of the volume fraction of  $N_2$  for the four models.

results from BP-ANN, RF and LS-SVM models yields a relative error within  $\pm 4.0\%$  for leakage rate measurement and  $\pm 3.4\%$  for  $N_2$  volume fraction measurement. These results are better than those from the three individual models. It is envisioned that the proposed method will provide a useful solution to the leakage detection in  $CO_2$  transportation pipeline networks for the practical deployment under CCS conditions.

#### CRedit authorship contribution statement

**Caiying Sun:** Writing – original draft, Validation, Methodology, Investigation. **Yong Yan:** Writing – review & editing, Supervision, Funding acquisition, Conceptualization. **Wenbiao Zhang:** Writing – review & editing, Supervision, Funding acquisition, Conceptualization. **Ding Shao:** Validation, Methodology, Investigation.

#### Declaration of competing interest

The authors declare that they have no known competing financial interests or personal relationships that could have appeared to influence the work reported in this paper.

#### Data availability

Data will be made available on request.

#### Acknowledgements

This work was supported by the National Natural Science Foundation of China (grant numbers 61973113 and 62073135) and the UK CCS Research Centre (www.ukccsrc.ac.uk). The UK CCSRC is funded by the EPSRC as part of the RCUK Energy Programme.

#### References

- [1] J. Blackford, H. Stahl, J. Bull, et al., Detection and impacts of leakage from sub-seafloor deep geological carbon dioxide storage, *Nat. Clim. Change* 4 (2014) 1011–1016, <https://doi.org/10.1038/nclimate2381>.
- [2] Z. Zhang, D. Huisingsh, Carbon dioxide storage schemes: technology, assessment and deployment, *J. Clean. Prod.* 142 (2017) 1055–1064, <https://doi.org/10.1016/j.jclepro.2016.06.199>.
- [3] J. Ma, L. Li, H. Wang, Y. Du, J. Ma, X. Zhang, Z. Wang, Carbon capture and storage: history and the road ahead, *Engineering* 14 (2022) 33–43, <https://doi.org/10.1016/j.eng.2021.11.024>.
- [4] L.H. Pham, R. Risza, A review of experimental and modelling methods for accidental release behaviour of high-pressurised  $CO_2$  pipelines at atmospheric environment, *Process Saf. Environ.* 104 (2016) 48–84, <https://doi.org/10.1016/j.psep.2016.08.013>.
- [5] H. Mahgerefteh, S. Brown, G. Denton, Modelling the impact of stream impurities on ductile fractures in  $CO_2$  pipelines, *Chem. Eng. Sci.* 74 (2012) 200–210, <https://doi.org/10.1016/j.ces.2012.02.037>.
- [6] Y. Yan, T. Borhani, S. Subraveti, et al., Harnessing the power of machine learning for carbon capture, utilisation, and storage (CCUS)—a state-of-the-art review, *Energ. Environ. Sci.* 14 (2021) 6122–6157, <https://doi.org/10.1039/d1ee02395k>.
- [7] Q. Hoarau, G. Ginolhac, A.M. Atto, J.M. Nicolas, Robust adaptive detection of buried pipes using GPR, *Signal Process.* 132 (2017) 293–305, <https://doi.org/10.1016/j.sigpro.2016.07.001>.
- [8] Y. Sun, L. Wei, C. Jiang, Z. Cong, Y. Wang, K. Cui, A. Ren, Acoustic microfiber sensor for gas pipeline leakage detection, *Measurement* 218 (2023), <https://doi.org/10.1016/j.measurement.2023.113242>.
- [9] J. Xie, Y. Zhang, Z. He, P. Liu, Y. Qin, Z. Wang, C. Xu, Automated leakage detection method of pipeline networks under complicated backgrounds by combining infrared thermography and Faster R-CNN technique, *Process Saf. Environ. Prot.* 174 (2023) 39–52, <https://doi.org/10.1016/j.psep.2023.04.006>.
- [10] H. Aslam, M.M. Mortula, S. Yehia, T. Ali, M. Kaur, Evaluation of the factors impacting the water pipe leak detection ability of GPR, infrared cameras, and spectrometers under controlled conditions, *Appl. Sci.-Basel.* 12 (2022) 1683, <https://doi.org/10.3390/app12031683>.
- [11] G. Zhang, S.C.M. Ho, L. Huo, J. Zhu, Negative pressure waves based high resolution leakage localization method using piezoceramic transducers and multiple temporal convolutions, *Sensors* 19 (2019) 1990, <https://doi.org/10.3390/s19091990>.
- [12] C. Zuo, X. Feng, Y.u. Zhang, L.u. Lu, J. Zhou, Crack detection in pipelines using multiple electromechanical impedance sensors, *Smart Mater. Struct.* 26 (2017), <https://doi.org/10.1088/1361-665X/aa7ef3>.
- [13] K. Ko, J. Lee, H. Chung, Highly efficient colorimetric  $CO_2$  sensors for monitoring  $CO_2$  leakage from carbon capture and storage sites, *Sci. Total Environ.* 729 (2020) 138786, <https://doi.org/10.1016/j.scitotenv.2020.138786>.
- [14] N. Nakamura, Y. Amao, Optical sensor for carbon dioxide combining colorimetric change of a pH indicator and a reference luminescent dye, *Anal. Bioanal. Chem.* 376 (2003) 642–646, <https://doi.org/10.1007/s00216-003-1949-3>.
- [15] M. Adegboye, W. Fung, A. Karnik, Recent advances in pipeline monitoring and oil leakage detection technologies: principles and approaches, *Sensors* 19 (2019) 2548, <https://doi.org/10.3390/s19112548>.
- [16] X. Cui, Y. Yan, Y. Ma, L. Ma, X. Han, Localization of  $CO_2$  leakage from transportation pipelines through low frequency acoustic emission detection, *Sens. Actuat. A-Phys.* 237 (2016) 107–118, <https://doi.org/10.1016/j.sna.2015.11.029>.
- [17] X. Cui, Y. Yan, M. Guo, X. Han, Y. Hu, Localization of  $CO_2$  leakage from a circular hole on a flat-surface structure using a circular acoustic emission sensor array, *Sensors* 16 (2016) 1951, <https://doi.org/10.3390/s16111951>.
- [18] F. Malcher, P. White, Acoustic monitoring techniques for subsea leak detection. A review of the literature, *NPL Rep. ac21* (2023), <https://doi.org/10.47120/npl.ac21>.
- [19] X. Cui, Y. Yan, Y. Hu, M. Guo, Performance comparison of acoustic emission sensor arrays in different topologies for the localization of gas leakage on a flat-surface structure, *Sens. Actuat. A-Phys.* 300 (2019) 111659, <https://doi.org/10.1016/j.sna.2019.111659>.
- [20] Y. Yan, X. Cui, M. Guo, X. Han, Localization of a continuous  $CO_2$  leak from an isotropic flat-surface structure using acoustic emission detection and near-field beamforming techniques, *Meas. Sci. Technol.* 27 (2016) 115105, <https://doi.org/10.1088/0957-0233/27/11/115105>.
- [21] T. Ishida, S. Desaki, Y. Kishimoto, M. Naoi, H. Fujii, Acoustic emission monitoring of hydraulic fracturing using carbon dioxide in a small-scale field experiment, *Int. J. Rock Mech. Min.* 141 (2021) 104712, <https://doi.org/10.1016/j.ijrmm.2021.104712>.
- [22] J. Kim, H. Yoon, S. Hwang, D. Jeong, S. Ki, B. Liang, H. Jeong, Real-time monitoring of  $CO_2$  transport pipelines using deep learning, *Process Saf. Environ.* 181 (2024) 480–492, <https://doi.org/10.1016/j.psep.2023.11.024>.
- [23] G. Skaugen, S. Roussanal, J. Jakobsen, A. Brunsfold, Techno-economic evaluation of the effects of impurities on conditioning and transport of  $CO_2$  by pipeline, *Int. J. Greenh. Gas Con.* 54 (2016) 627–639, <https://doi.org/10.1016/j.ijggc.2016.07.025>.
- [24] F. Zanolletti, S. Martynov, V. Cozzani, H. Mahgerefteh, Multi-objective economic and environmental assessment for the preliminary design of  $CO_2$  transport pipelines, *J. Clean. Prod.* 411 (2023) 137330, <https://doi.org/10.1016/j.jclepro.2023.137330>.
- [25] Y. Choi, S. Nestic, D. Young, Effect of impurities on the corrosion behavior of  $CO_2$  transmission pipeline steel in supercritical  $CO_2$ -water environments, *Environ. Sci. Tech.* 44 (2010) 9233–9238, <https://doi.org/10.1021/es102578c>.

- [26] X. Guo, X. Yan, J. Yu, et al., Pressure responses and phase transitions during the release of high pressure CO<sub>2</sub> from a large-scale pipeline, *Energy* 118 (2017) 1066–1078, <https://doi.org/10.1016/j.energy.2016.10.133>.
- [27] S.K. Mahjour, S.A. Faroughi, Risks and uncertainties in carbon capture, transport, and storage projects: a comprehensive review, *Gas Sci. Eng.* (2023) 205117, <https://doi.org/10.1016/j.jgsce.2023.205117>.
- [28] C. Wang, Y. Li, L. Teng, et al., Experimental study on dispersion behavior during the leakage of high pressure CO<sub>2</sub> pipelines, *Exp. Therm Fluid Sci.* 105 (2019) 77–84, <https://doi.org/10.1016/j.expthermflusci.2019.03.014>.
- [29] X. Zhou, K. Li, R. Tu, J. Yi, Q. Xie, X. Jiang, A modelling study of the multiphase leakage flow from pressurised CO<sub>2</sub> pipeline, *J. Hazard. Mater.* 306 (2016) 286–294, <https://doi.org/10.1016/j.jhazmat.2015.12.026>.
- [30] A.H. El-Kady, M.T. Amin, F. Khan, M.M. El-Halwagi, Analysis of CO<sub>2</sub> pipeline regulations from a safety perspective for offshore carbon capture, utilization, and storage (CCUS), *J. Clean. Prod.* (2024) 140734, <https://doi.org/10.1016/j.jclepro.2024.140734>.
- [31] H.A. Baroudi, A. Awoyomi, K. Patchigolla, K. Jonnalagadda, E.J. Anthony, A review of large-scale CO<sub>2</sub> shipping and marine emissions management for carbon capture, utilisation and storage, *Appl. Energ.* 287 (2021) 116510, <https://doi.org/10.1016/j.apenergy.2021.116510>.
- [32] S. Yu, X. Yan, Y. He, et al., Study on the decompression behavior during large-scale pipeline puncture releases of CO<sub>2</sub> with various N<sub>2</sub> compositions: experiments and mechanism analysis, *Energy* (2024) 131180, <https://doi.org/10.1016/j.energy.2024.131180>.
- [33] N. Nabipour, S. Qasem, E. Salwana, A. Baghban, Evolving LSSVM and ELM models to predict solubility of non-hydrocarbon gases in aqueous electrolyte systems, *Measurement* 164 (2020) 107999, <https://doi.org/10.1016/j.measurement.2020.107999>.
- [34] D. Shao, Y. Yan, W. Zhang, S. Sun, L. Xu, Dynamic measurement of gas volume fraction in a CO<sub>2</sub> pipeline through capacitive sensing and data driven modelling, *Int. J. Greenh. Gas Con.* 94 (2019) 102950, <https://doi.org/10.1016/j.ijggc.2019.102950>.
- [35] C. Sun, L. Wang, Y. Yan, W. Zhang, D. Shao, A novel heterogeneous ensemble approach to variable selection for gas-liquid two-phase CO<sub>2</sub> flow metering, *Int. J. Greenh. Gas Con.* 110 (2021) 103418, <https://doi.org/10.1016/j.ijggc.2021.103418>.
- [36] S. Miraboutalebi, P. Kazemi, P. Bahrami, Fatty acid methyl ester (FAME) composition used for estimation of biodiesel cetane number employing random forest and artificial neural networks: a new approach, *Fuel* 166 (2016) 143–151, <https://doi.org/10.1016/j.fuel.2015.10.118>.
- [37] M. Li, M. Wang, R. Ding, T. Deng, S. Fang, F. Lai, R. Luoi, Study of acoustic emission propagation characteristics and energy attenuation of surface transverse wave and internal longitudinal wave of wood, *Wood Sci. Technol.* 55 (2021) 1619–1637, <https://doi.org/10.1007/s00226-021-01329-y>.
- [38] L. Duehee, R. Baldick, Future wind power scenario synthesis through power spectral density analysis, *IEEE T Smart Grid.* 5 (2014) 490–500, <https://doi.org/10.1109/TSG.2013.2280650>.
- [39] Z. Bei, Z. Yu, N. Luo, C. Jiang, C. Xu, S. Feng, Configuring in-memory cluster computing using random forest, *Fut. Gener. Comp. Sy.* 79 (2018) 1–15, <https://doi.org/10.1016/j.future.2017.08.011>.
- [40] ISO 27913: Carbon Dioxide Capture, Transportation and Geological Storage-Pipeline Transportation Systems, International Organization for Standardization (ISO), 2016, <https://www.iso.org/obp/ui/#iso:std:iso:27913:ed-1:v1:en> (2016).
- [41] ISO/TR 27921:2020 Carbon Dioxide Capture, Transportation, and Geological Storage-Cross Cutting issues-CO<sub>2</sub> Stream Composition, International Organization for Standardization, Geneva, Switzerland, 2020, <https://www.iso.org/standard/67273.html>.
- [42] GB/T 42797-2023, Carbon Dioxide Capture, Transportation and Geological Storage-Pipeline Transportation Systems. National Standardization Administration, 2023.